PCCP

PAPER

Patchy worm-like micelles: solution structure studied by small-angle neutron scattering

Sabine Rosenfeldt,[a] Frank Lüdel,[b] Christoph Schulreich,[b] Thomas Hellweg,*[b] Aurel Radulescu,[c] Joachim Schmelz,[d] Holger Schmalz[d] and Ludger Harnau*[ef]

Triblock terpolymers exhibit a rich self-organization behavior including the formation of fascinating cylindrical core–shell structures with a phase separated corona. After crystallization-induced self-assembly of polystyrene-*block*-polyethylene-*block*-poly(methyl methacrylate) triblock terpolymers (abbreviated as SEMs = Styrene-Ethylene-Methacrylates) from solution, worm-like core–shell micelles with a patchy corona of polystyrene and poly(methyl methacrylate) were observed by transmission electron microscopy. However, the solution structure is still a matter of debate. Here, we present a method to distinguish *in situ* between a Janus-type (two faced) and a patchy (multiple compartments) configuration of the corona. To discriminate between both models the scattering intensity must be determined mainly by one corona compartment. Contrast variation in small-angle neutron scattering enables us to focus on one compartment of the worm-like micelles. The results validate the existence of the patchy structure also in solution.

1 Introduction

Block copolymers exhibit a rich and fascinating self-assembly behavior in bulk and in selective solvents.[1–4] A lot of the occuring structures are promising for applications in drug delivery, optoelectronics or as scaffolds for nanoparticle assembly.[5–10] Choosing the block length and the proper solvent conditions a huge variety of different structures can be generated.[11]

Many of the solution-based assemblies can be summarized under the term multicompartment micelles. Similar to proteins, multicompartment micelles combine different physical nano-environments in well-segregated compartments and exhibit a rich phase behavior including remarkably complex self-assemblies. They show a compartmentalization either of the core or the corona.[12–15] Surface-compartmentalized particles exhibit useful features for several applications, *e.g.*, the formation of hierarchically ordered superstructures, the use as potential scaffolds for the directed incorporation of metallic nanoparticles or as surfactants and emulsifiers.[16–20] Regarding corona-compartmentalized structures, Janus particles[16,21] have been formed by template-assisted approaches while solution self-assembly mostly results in patchy particles,[20,22,23] *i.e.*, structures with more than two surface compartments. Whereas there are well-known examples for one-dimensional structures with compartmentalized cores[12] or a Janus-like corona,[24,25] the majority of patchy particles are spherical in nature. Even though theoretical simulations by Binder *et al.* suggest the existence of one-dimensional nanostructures with patch-like compartmentalization of the corona,[26–28] only a few examples have actually been published. For example, Liu *et al.* produced cylindrical micelles by dialysis of a triblock terpolymer against selective solvents that are able to further organize to double and triple helices.[30]

In recent years, a new way of synthesizing stable anisotropic particles exploiting block copolymers with one crystallizable block moved into the focus of several research groups.[29] Among these, polyferrocenylsilane containing block copolymers have been investigated most intensively, revealing a multitude of unprecedented structures, such as block *co*-micelles, scarf-like micelles and supramolecular brush layers.[31–33] The solution self-assembly of these crystalline-coil block copolymers is controlled by temperature or by the addition of a non-solvent for the crystallizable block, which induces crystallization. Especially, cylindrical or worm-like micelles with high aspect ratios have raised interest in bioscience and materials science.[29,34]

Recently, we have developed the preparation of worm-like crystalline core micelles with a patchy corona from semi-crystalline

[a] Physikalische Chemie I, Universität Bayreuth, D-95440 Bayreuth, Germany
[b] Physikalische und Biophysikalische Chemie (PC III), Universität Bielefeld, D-33615 Bielefeld, Germany. E-mail: thomas.hellweg@uni-bielefeld.de
[c] Jülich Centre for Neutron Science JCNS, Forschungszentrum Jülich GmbH, Outstation at FRM II, Lichtenbergstraße 1, 85747 Garching, Germany
[d] Makromolekulare Chemie II, Universität Bayreuth, D-95440 Bayreuth, Germany
[e] Max-Planck-Institut für Intelligente Systeme, Heisenbergstrasse 3, D-70569 Stuttgart, Germany
[f] Institut für Theoretische und Angewandte Physik, Universität Stuttgart, Pfaffenwaldring 57, D-70569 Stuttgart, Germany. E-mail: harnau@fluids.mpi-stuttgart.mpg

polystyrene-*block*-polyethylene-*block*-poly(methyl methacrylate) (SEM) triblock terpolymers in organic solvents. Our method provides a straightforward bottom-up strategy for building up one-dimensional patchy nanostructures *via* crystallization-induced self-assembly. The structure formation is triggered simply by a decrease in temperature that induces crystallization of the polyethylene (PE) middle block.[35,36] Transmission electron microscopy revealed that the corona exhibits a patchy structure made of microphase-separated polystyrene (PS) and poly(methyl methacrylate) (PMMA) enclosing the crystalline PE core. The complexity of surface-compartmentalized nanostructures complicates the determination of the morphology and dimensions. Up to now, morphological information has been obtained by imaging techniques that usually were applied to dried samples. To get a deeper insight into dissolved worm-like crystalline core micelles, scattering methods such as small-angle neutron scattering are powerful tools as has been shown for worm-like or Janus-type structures by Fütterer *et al.*[37] and by Walther *et al.*,[38] respectively. Here, we present the first *in situ* shape sensitive investigation of patchy worm-like micelles from a SEM triblock terpolymer. To achieve this goal, a theoretical model for these complex structures is developed and experimentally verified by small-angle neutron scattering on patchy worm-like crystalline core micelles containing deuterated polystyrene blocks (dSEM) at a selected contrast.

2 Experimental section

2.1 Synthesis and sample preparation

The dSEM triblock terpolymer was obtained by catalytic hydrogenation of the corresponding dSBM (B = poly(1,4-butadiene)) triblock terpolymer precursor synthesized by sequential anionic polymerization. The polystyrene block of the precursor was fully deuterated. The composition of the dSBM precursor is determined to be $S_{47d}B_{24}M_{29}^{85}$ by a combination of MALDI-TOF and ^{1}H-NMR, which results in $S_{47d}E_{24}M_{29}$ after hydrogenation (subscripts denote the mass fraction in percent, the superscript gives the overall molecular weight in kg per mol, and d indicates that the PS block is fully deuterated). The formula of the investigated $S_{47d}E_{24}M_{29}^{86}$ can also be expressed in terms of the number of monomer units and would read $S_{359d}E_{747}M_{250}$. Full saturation of the double bonds was confirmed by ^{1}H-NMR in deuterated toluene at 65 °C. A detailed description of the synthesis of the SEM terpolymer is given in the literature.[35] Micelles of $S_{47d}E_{24}M_{29}^{86}$ are formed by crystallization induced self-assembly upon cooling.[36] As the polyethylene block in a 10 g L^{-1} solution melts at a peak melting temperature T_m = 45 °C and crystallizes at T_c = 21 °C, the solutions for the scattering experiments were prepared as follows: to eliminate any influence of thermal history, 10 g L^{-1} of the dSEM were dissolved in the corresponding solvent, *e.g.*, in tetrahydrofuran (THF) or a mixture of protonated and deuterated THF (deuteration degree 99.5%, Deutero GmbH) at 65 °C. After 1 h the solutions were quenched down to 20 °C in a water-bath and equilibrated for two days.

2.2 Small-angle neutron scattering (SANS)

The SANS data were obtained using the KWS 1 instrument at the FRM II in Munich, Germany. The raw data were corrected for background, solvent and empty cell scattering by the use of the software provided by the Jülich Center for Neutron Science (JCNS) at the FRM II. Absolute intensities were obtained by using a calibrated reference scatterer. For all data sets, the rate of incoherent scattering caused by the protons was determined at high scattering vector, set as a constant and subtracted from the raw data.

2.3 Transmission electron microscopy (TEM)

For TEM studies the solutions were diluted to 1 g L^{-1}. Samples were prepared by placing a drop of the solution on a carbon-coated copper grid. After 20 s, excess solution was removed by blotting with a filter paper. Subsequently, elastic bright-field TEM was performed on a Zeiss 922 OMEGA EFTEM (Zeiss NTS GmbH, Oberkochen, Germany) operated at 200 kV. Staining was performed with RuO_4 vapor for at least 20 min. RuO_4 is known to selectively stain PS, which enables to distinguish between PS and PMMA domains in the corona of the micelles.

3 Results and discussion

3.1 TEM micrographs

Recently, the formation of worm-like crystalline core micelles with a patch-like corona from a polystyrene-*block*-polyethylene-*block*-poly(methyl methacrylate) triblock terpolymer was reported.[35,36] 2D ^{1}H-NMR NOESY techniques applied to a $S_{39}E_{21}M_{40}^{91.5}$ in toluene pointed to a micro phase-separation of the corona.[35] However, this technique is not able to distinguish between a Janus-type (two-faced) or a patchy (multiple PS and PMMA compartments) configuration of the corona. Hence, the assumption of a patchy worm-like structure in solution was based on TEM studies. Fig. 1 shows a TEM micrograph of the structures formed by quenching a solution of $S_{47d}E_{24}M_{29}^{86}$ from 65 °C to 20 °C. In order to distinguish the different compartments in the corona in the dried state, the PS domains were stained with RuO_4. The TEM micrographs clearly exhibit similar patch-like compartments of the corona both in THF (see Fig. 1(a)) and in deuterated THF (see Fig. 1(b)). Hence, a change in the corona structure due to isotope effects of the solvent can be ruled out. In many sections an alternating array of the PS patches along the core of the worm-like crystalline core micelles is observed. THF is a good solvent for both PS and PMMA and the adopted random-coil configuration of the chains results in different dimensions of the hemi-shells. A detailed discussion about TEM and cryo-TEM studies on worm-like crystalline core micelles formed by SEM terpolymers can be found elsewhere.[35,36]

3.2 Solution structures as obtained from SANS

Scattering techniques provide knowledge about the solution structure without perturbing the sample. Moreover, in the case of neutron scattering, contrast variation using deuterated monomers reveals details of the internal structure in a unique way. SANS data taken at highest contrast between solvent and
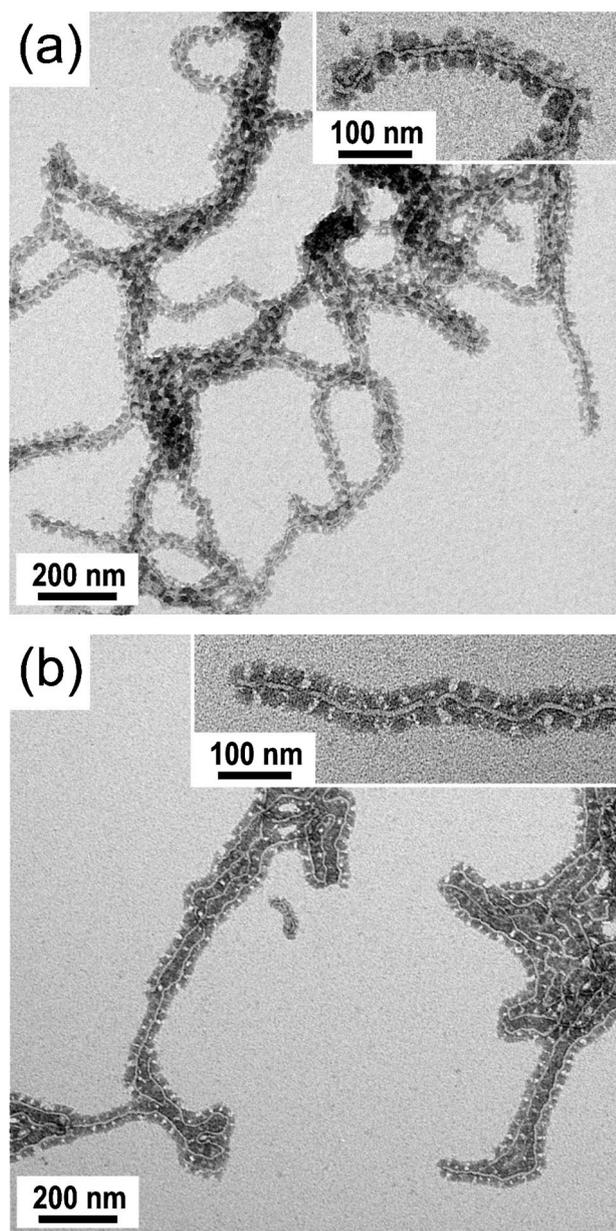
Fig. 1 TEM micrographs of the self-assembled structure of $S_{47d}E_{24}M_{29}^{86}$ (1 g L^{-1}) in THF (a) and deuterated THF (b). The PS domains are stained with RuO$_4$ and therefore visible as dark gray areas.

solute are used to explore the shape of the entire species. At intermediate and low contrast local details of the self-assembled structures can be detected. The scattering intensities of such a contrast series can be interpreted by applying models with appropriate geometry and scattering length density distribution.[38–42]

3.2.1 Scattering intensity. SANS determines the scattering intensity $I(\boldsymbol{q})$ as a function of the scattering vector $\boldsymbol{q}$ and the concentration of the dissolved particles. In addition to the coherent scattering intensity $I_{\mathrm{coh}}(\boldsymbol{q})$, there is always an incoherent contribution I_{incoh} that is due to the protons present in the particles under consideration. The scattering intensity can be written as

$$I(\boldsymbol{q}) = I_{\mathrm{coh}}(\boldsymbol{q}) + I_{\mathrm{incoh}}. \qquad (1)$$

Note that in the notation the dependence on the concentration of the dissolved particles is suppressed. The $\boldsymbol{q}$-independent incoherent contribution I_{incoh} of individual particles must be subtracted carefully from experimental data in order to obtain meaningful results on the structure and interaction of the dissolved particles.[41] Due to the mesoscopic scale of the particles, the solvent will be modeled as structureless continuum providing a homogeneous scattering length density b_{solvent}.

In order to take into account particle polydispersity we consider a multicomponent system involving ν species of particles with particle numbers N_{O} ($1 \leq \mathrm{O} \leq \nu$) in the volume V. Each particle of a species O carries n_{O} scattering units. In the case of the triblock terpolymer micelles under consideration, it proves convenient to assign an index j ($1 \leq j \leq n_{\mathrm{O}}$) to scattering units, and to order them such that units $1 \leq j \leq n_{\mathrm{O}}^{(\mathrm{E})}$ belong to the compound PE, $n_{\mathrm{O}}^{(\mathrm{E})} + 1 \leq j \leq n_{\mathrm{O}}^{(\mathrm{E})} + n_{\mathrm{O}}^{(\mathrm{M})}$ belong to the compound PMMA, and $n_{\mathrm{O}}^{(\mathrm{E})} + n_{\mathrm{O}}^{(\mathrm{M})} + 1 \leq j \leq n_{\mathrm{O}}$ belong to the compound PS. The coherent contribution to the scattering intensity in the ν-component system is given by

$$I_{\mathrm{coh}}(\boldsymbol{q}) = \sum_{\mathrm{O,P}=1}^{\nu} I_{\mathrm{OP}}(\boldsymbol{q}), \qquad (2)$$

with the partial scattering intensities

$$I_{\mathrm{OP}}(\boldsymbol{q}) = \frac{1}{V} \left\langle \sum_{j=1}^{n_{\mathrm{O}}} \sum_{k=1}^{n_{\mathrm{P}}} \sum_{\alpha=1}^{N_{\mathrm{O}}} \sum_{\gamma=1}^{N_{\mathrm{P}}} \Delta \tilde{b}_{j\mathrm{O}}^{(\alpha)} \Delta \tilde{b}_{k\mathrm{P}}^{(\gamma)} \mathrm{e}^{\mathrm{i}\boldsymbol{q} \cdot \left(\boldsymbol{r}_{j\mathrm{O}}^{(\alpha)} - \boldsymbol{r}_{k\mathrm{P}}^{(\gamma)} \right)} \right\rangle. \quad (3)$$

Here, $\boldsymbol{r}_{j\mathrm{O}}^{(\alpha)}$ is the position vector of the jth scattering unit of the αth particle of species O. The difference in the scattering length of this scattering unit and the average scattering length of the solvent is denoted as $\Delta \tilde{b}_{j\mathrm{O}}^{(\alpha)}$, and $\langle \rangle$ denotes an ensemble average. It proves convenient to decompose the partial scattering intensities according to

$$I_{\mathrm{OP}}(\boldsymbol{q}) = \rho_{\mathrm{O}} \omega_{\mathrm{O}}(\boldsymbol{q}) \delta_{\mathrm{OP}} + \rho_{\mathrm{O}} \rho_{\mathrm{P}} h_{\mathrm{OP}}(\boldsymbol{q}), \qquad (4)$$

where

$$h_{\mathrm{OP}}(\boldsymbol{q}) = \frac{V}{N_{\mathrm{O}} N_{\mathrm{P}}} \left\langle \sum_{j=1}^{n_{\mathrm{O}}} \sum_{k=1}^{n_{\mathrm{P}}} \sum_{\alpha=1}^{N_{\mathrm{O}}} \sum_{\substack{\gamma=1 \\ \gamma \neq \alpha}}^{N_{\mathrm{P}}} \Delta \tilde{b}_{j\mathrm{O}}^{(\alpha)} \Delta \tilde{b}_{k\mathrm{P}}^{(\gamma)} \mathrm{e}^{\mathrm{i}\boldsymbol{q} \cdot \left(\boldsymbol{r}_{j\mathrm{O}}^{(\alpha)} - \boldsymbol{r}_{k\mathrm{P}}^{(\gamma)} \right)} \right\rangle. $$

$$(5)$$

is a particle-averaged total correlation function for pairs of particles of species O and P. The number density of particles of species O is designated as $\rho_{\mathrm{O}} = N_{\mathrm{O}}/V$. The particle-averaged intramolecular correlation function

$$\omega_{\mathrm{O}}(\boldsymbol{q}) = \frac{1}{N_{\mathrm{O}}} \left\langle \sum_{j=1}^{n_{\mathrm{O}}} \sum_{k=1}^{n_{\mathrm{P}}} \sum_{\alpha=1}^{N_{\mathrm{O}}} \Delta \tilde{b}_{j\mathrm{O}}^{(\alpha)} \Delta \tilde{b}_{k\mathrm{O}}^{(\alpha)} \mathrm{e}^{\mathrm{i}\boldsymbol{q} \cdot \left(\boldsymbol{r}_{j\mathrm{O}}^{(\alpha)} - \boldsymbol{r}_{k\mathrm{O}}^{(\alpha)} \right)} \right\rangle \qquad (6)$$

characterizes the scattering length distribution, and hence also the geometric shape of particles of species O. While the particle-averaged intramolecular correlation functions account for the interference of radiation scattered from different parts of individual particles in a scattering experiment, the local order in the fluid is characterized by the total correlation functions. For flexible particles the intramolecular correlation functions depend on the particle number density and follow from a statistical average over particle configurations.

As suggested by the imaging data (see Fig. 1), the triblock terpolymer micelles may be considered as worm-like core–shell cylinders with phase-separated shells. In the scattering vector regime of a SANS experiment both the contour length and the persistence length cannot be resolved for rather long and stiff cylindrical particles.[41,44] As a prerequisite for the following analysis we have confirmed that the scattering intensity of a homogeneous weakly bendable cylinder with the same configuration as the triblock terpolymer micelle shown in the inset of Fig. 1(b) is nearly indistinguishable from the scattering intensity of a corresponding homogeneous rigid cylinder in the scattering vector regime accessible by SANS. Hence, only the scattering intensity of rigid cylinders is considered in the analysis of the SANS experiments. In the limit of a continuous distribution of scattering units, the intramolecular correlation function of randomly oriented core–shell cylinders is given by

$$\omega_O(q) = \frac{1}{4\pi} \int_0^{2\pi} d\phi \int_0^{\pi} d\theta \sin\theta \, F_O(q,\theta,\phi) F_O^*(q,\theta,\phi) \quad (7)$$

with

$$F_O(q,\theta,\phi) = \int_{-L/2}^{L/2} dz \int_0^{\infty} dr \, r \int_0^{2\pi} d\phi_r \Delta b_O(r,\phi_r,z) e^{i\boldsymbol{q}\cdot\boldsymbol{r}}. \quad (8)$$

Here, $\boldsymbol{q} = q(\sin\theta\cos\phi, \sin\theta\sin\phi, \cos\theta)$ is the scattering vector described by spherical coordinates and $\boldsymbol{r} = (r\cos\phi_r, r\sin\phi_r, z)$ denotes the position vector of a scattering unit of an individual core–shell cylinder described by cylindrical coordinates. The origin of the coordinates is taken to be the center of the cylinder of length L and $\Delta b_O(r,\phi_r,z)$ denotes the scattering length density function, which specifies the internal structure of an individual core–shell cylinder. For the triblock terpolymer micelles the index O in eqn (2), (4), (7), and (8) allows one to take into account polydispersity of the scattering length density function.

3.2.2 Janus type and patchy cylinders. As Fig. 2 illustrates, the cylinders are characterized by a core–shell structure with a PE core of radius R_E marked in gray and a biphasic PS-PMMA shell consisting of regions of unlike size and scattering length densities shown in blue and red. Hence, the scattering length density function equals Δb_E, Δb_S, and Δb_M in the regions marked in gray, blue, and red, respectively. More specifically, two shell patterns will be distinguished. (i) Fig. 2(a): a Janus-type architecture, *i.e.*, the shell consists of two homogeneous hemi-shells which might have different or similar extensions (R_S and R_M) and unlike scattering length densities. (ii) Fig. 2(b): the two inhomogeneous hemi-shells consist of alternating regions of scattering length densities. Here, D_S and D_M describe the lengths of the alternating regions of the so-called patchy cylinder. Fig. 3(a) displays scattering intensities for noninteracting ($h_{OP}(\boldsymbol{q}) = 0$) and monodisperse ($\nu = 1$) cylinders of length $L = 425.5$ nm and radii $R_E = 4.3$ nm, $R_M = 15.5$ nm, $R_S = 22.0$ nm as calculated from eqn (1)–(8). The dashed lines show the results for Janus cylinders (see Fig. 2(a)), while the solid lines represent the scattering intensities of patchy cylinders (see Fig. 2(b)) with $D_M = D_S = 22.4$ nm. All scattering intensities
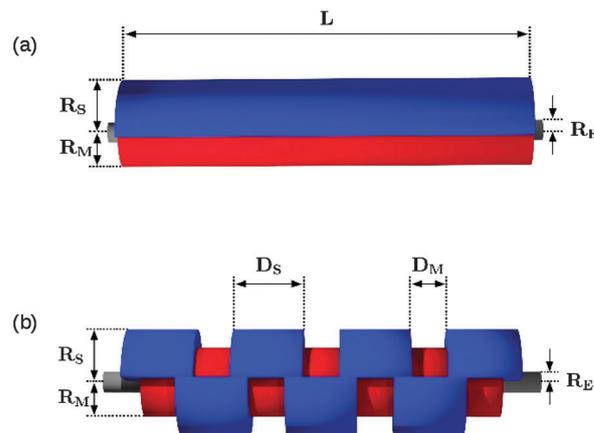

Fig. 2 Illustrations of two possible architectures of micro phase-separated shells of cylindrical particles. The cylinders are characterized by a core–shell structure with a PE core of radius R_E marked in gray and a biphasic PS-PMMA shell consisting of regions of unlike size and scattering length densities marked in blue and red. In the main text the cylindrical particles are denoted as Janus cylinders (a) and patchy cylinders (b).

are normalized to the volume fraction $\phi = \rho_O/V_O$, where V_O is the particle volume. Moreover, the ratio of the scattering length density differences of PS and PE is $\Delta b_S/\Delta b_E = -0.751$, where $\Delta b_E = b_{solvent} - b_E$ and $b_E = -0.34 \times 10^{10}$ cm^{-2} are the scattering length densities of the solvent and PE, respectively. For comparison, three values of the ratio of the scattering length density differences of PS and PMMA $\Delta b_S/\Delta b_M$ are considered, where $\Delta b_S/\Delta b_M = 6.859$ (data set in the middle) corresponds to PS and PMMA in THF$_H$. The scattering intensities shown in Fig. 3(a) have the following features. They exhibit the q^{-1} scaling relation (short dotted line) for small scattering vectors which is characteristic for the linear arrangement of scattering units along the main axis of a cylinder. For the patchy cylinders (solid lines), the scattering intensity exhibits a minimum at $q \approx 0.14$ nm^{-1}, while for the Janus cylinders no minimum is observed, provided $\Delta b_S/\Delta b_M \gtrsim 6.859/3$. From the figure it is apparent that the existence or absence of a minimum of the scattering intensity at intermediate scattering vectors allows one to distinguish Janus cylinders from patchy cylinders provided the ratio of two scattering length density differences of the biphasic shell is sufficiently large. In addition we note that the scattering intensity of a homogeneous cylinder of similar size does not exhibit a minimum at $q \approx 0.14$ nm^{-1} as is apparent from the lower dotted line in Fig. 3(a).

In Fig. 3(b) the experimental scattering intensity of the triblock terpolymer micelles in pure THF$_H$ is compared to the calculated results for noninteracting patchy cylinders. For the morphological study this contrast condition is well suited due to the fact that the scattering pattern mainly is determined by the deuterated PS patch of the shell. The model parameters are the same as for the solid middle line in Fig. 3(a) except for the lengths of the alternating regions of the shell which are given by $D_M = 14.0$ nm and $D_S = 29.0$ nm. Hence we take into account that the size of the PMMA block (M$_{29}$) characterized by D_M, R_M is smaller than the size of the PS block (S$_{47d}$) characterized by D_S, R_S. The ratio of the size of the
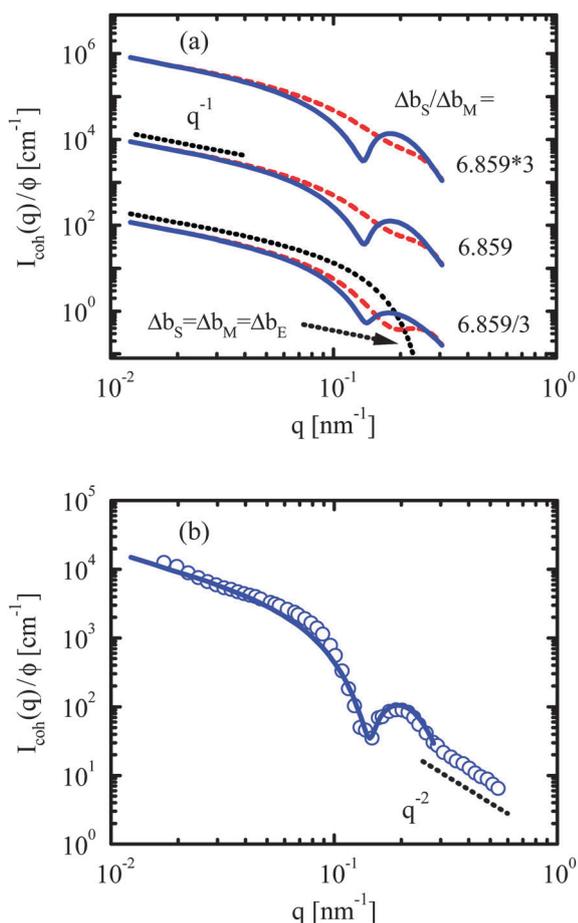
Fig. 3 (a) Comparison of the scattering intensity $I_{coh}(\boldsymbol{q})/\phi$ of Janus cylinders (dashed lines, see Fig. 2(a)) with the scattering intensity of patchy cylinders (solid lines, see Fig. 2(b)) with $D_M = D_S = 22.4$ nm. The curves have been calculated according to eqn (1)–(8) with $h_{OP}(\boldsymbol{q}) = 0$ and $\nu = 1$, *i.e.*, for noninteracting and monodisperse cylinders. The remaining model parameters are given by $L = 425.5$ nm, $R_E = 4.3$ nm, $R_M = 15.5$ nm, $R_S = 22.0$ nm, $\Delta b_S/\Delta b_E = -0.751$ and $\Delta b_E = 0.52 \times 10^{10}$ cm^{-2}. Moreover, the ratio of the scattering length density difference of PS and PMMA decreases from top to bottom according to $\Delta b_S/\Delta b_M = 6.859 \times 3$, 6.859, 6.859/3, where the value 6.859 corresponds to the actual experimental system discussed in panel (b). In addition the lower dotted line depicts the scattering intensity of a homogeneous cylinder with $\Delta b_S/\Delta b_E = \Delta b_S/\Delta b_M = 1$ and $R_M = R_S = 15.5$ nm. For clarity, the upper and lower data sets have been shifted up and down, respectively, by a factor of 10^2. (b) Measured scattering intensity of the triblock terpolymer micelles (10 g L^{-1}) in THF$_H$ (symbols) together with the calculated results for noninteracting patchy cylinders (solid line). The model parameters are the same as for the solid middle line in panel (a) except for $D_M = 14.0$ nm and $D_S = 29.0$ nm. The short dotted lines in panels (a) and (b) represent two asymptotic scaling laws as discussed in the main text.

three-dimensional patches $D_S(R_S^2 - R_E^2)/(D_M(R_M^2 - R_E^2)) = 4.35$ is similar to the cube of the ratio of the mass fractions of the one-dimensional PS and PMMA chains $(47/29)^3 = 4.26$. From the figure it is apparent that the experimentally determined scattering intensity (symbols) exhibits a pronounced minimum at $q \approx 0.14$ nm^{-1} which is characteristic for a patchy cylinder as discussed above. The deviations between the experimental data and the calculated results (solid line) for

intermediate scattering vectors $q \in [0.03, 0.1]$ are due to the fact that the PS and PMMA blocks do not form perfect patchy half-cylinders as is assumed in the model shown in Fig. 2(b). Nevertheless, the combination of Fig. 3(a) and (b) demonstrates that patchy triblock terpolymer micelles are indeed present in THF$_H$. For comparison we emphasize that experimentally determined scattering intensities of Janus cylinders do not exhibit minima at intermediate scattering vectors in agreement with the calculated results shown in Fig. 3(a).[38]

Although eqn (7) and (8) have been derived for a rigid cylinder of a definite shape illustrated in Fig. 2, in reality concentration fluctuations of the PS and PMMA polymer chains contribute to the scattering intensity. On the basis of our experience with various polymer nanoparticles[43–46] we expect that the contribution of the polymer concentration fluctuations becomes important for large scattering vectors $q \gtrsim 0.3$ nm^{-1}. Within a Gaussian approximation the scaling relation $I_{coh}(\boldsymbol{q}) \sim q^{-2}$ is valid for large scattering vectors as indicated by the dotted line in Fig. 3(b). Moreover, we have confirmed that moderate size polydispersity (*e.g.*, $D_S = 29.0 \pm 3.0$ nm) does not lead to pronounced changes of the calculated scattering intensity. Therefore, one may consider a monodisperse model system as an appropriate approximation.

3.2.3 Contrast variation. Fig. 4(a) displays SANS intensities of the triblock terpolymer micelles in different THF$_D$: THF$_H$ mixtures corresponding to different scattering length densities of the solvent (symbols). Such a contrast variation allows consistency checks of the theoretical modeling because the contribution of the three polymers PE, PMMA, and PS to the scattering intensity depends sensitively on the scattering length density of the solvent. The figure demonstrates that varying the scattering length contrast leads to marked differences in the scattering intensities. In particular, the minima of the scattering intensities of the lower two data sets disappear upon increasing the scattering length density of the solvent (upper three data sets) due to an increasing contribution of PE to the scattering intensity. The pronounced minima reflect the phase-separated shell of patchy cylinders (see Fig. 2(b)) while the homogeneous PE core cylinder does not lead to a minimum in this scattering vector regime.

The dashed lines in Fig. 4(a) show the calculated results for noninteracting patchy cylinders using the same model parameters as in Fig. 3(b). Some features of the measured scattering intensities such as the disappearance of the minimum upon increasing the scattering length density of the solvent are captured by the theoretical approach. However, the calculated results for noninteracting patchy cylinders and the experimental data deviate due to interactions between the micelles. The concentration 10 g L^{-1} is ten times higher than the one used for the TEM micrographs shown in Fig. 1. This rather high polymer concentration was necessary in order to obtain a good signal-to-noise ratio. We emphasize that neither modeling the cores of the elongated micelles as one-dimensionally connected objects such as worm-like or helical-like chains nor taking into account the semicrystallinity of PE[47] leads to a peak of the scattering intensities at $q \approx 0.1$ nm^{-1} in the cases of dominating contributions of PE to the scattering intensities (upper three data sets in Fig. 4(a)). In order to justify the
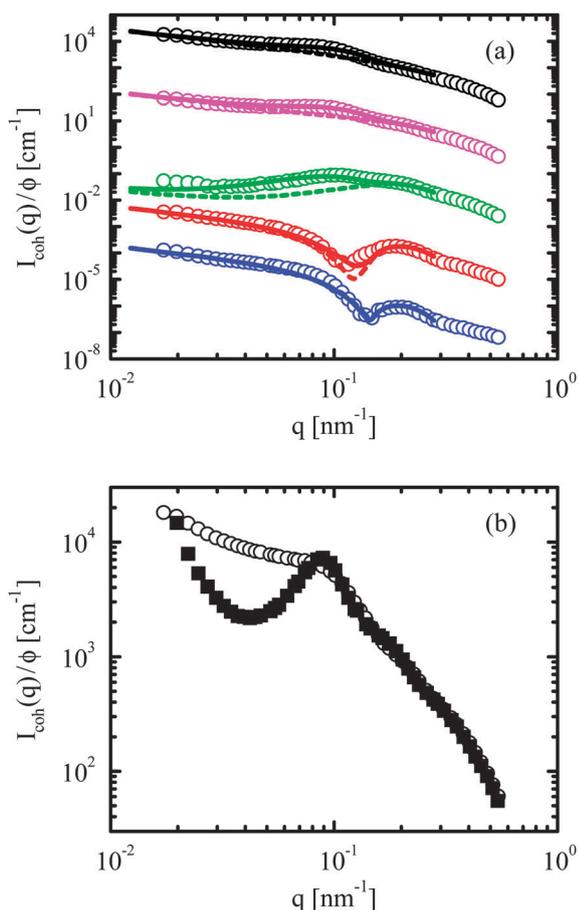
Fig. 4 (a) Measured scattering intensity $I_{coh}(\boldsymbol{q})/\phi$ of the triblock terpolymer micelles at concentration 10 g L^{-1} (symbols). The scattering length densities of the solvent increases from bottom to top ($b_{solvent}$ = 0.18, 1.36, 3.23, 5.13, 6.32 × 10^{10} cm^{-2}) while the corresponding ratios of the scattering length density differences of the micelles are given by $\Delta b_S/\Delta b_M$ = 6.859, −19.731, −1.531, −0.337, −0.033 and $\Delta b_S/\Delta b_E$ = −0.751, −0.187, −0.057, −0.015, −0.002, with $\Delta b_E = b_{solvent} - b_E$ and b_E = −0.34 × 10^{10} cm^{-2}. The four lower scattering intensities are shifted down by a factor of 10^2, 10^4, 10^6, 10^8, respectively. The dashed lines represent calculated results for noninteracting ($h_{OP}(\boldsymbol{q})$ = 0) patchy cylinders using the same model parameters as in Fig. 3(b). In the case of the solid lines a contribution of the total correlation function $h_{OP}(\boldsymbol{q})$ to the scattering intensity is taken into account. For the lowest scattering length density of the solvent the solid line is nearly indistinguishable from the dashed line. (b) Comparison of the normalized measured scattering intensity of the triblock terpolymer micelles at concentration 10 g L^{-1} (open circles) with the corresponding data at 40 g L^{-1} (solid squares) in fully deuterated THF ($b_{solvent}$ = 6.32 × 10^{10} cm^{-2}). The differences between the open and solid symbols reflect pair correlations between the micelles.

argumentation based on our additional calculations of various intramolecular correlation functions, we have performed a scattering experiment for an even higher micelle concentration 40 g L^{-1} in fully deuterated THF (solid squares in Fig. 4(b)). Indeed the observed peak of the scattering intensity is more pronounced as compared to the one for 10 g L^{-1} (open circles in Fig. 4(b)) due to increased interparticular correlations. This interpretation is consistent with the observation that the 40 g L^{-1} sample was rather viscous whereas the 10 g L^{-1}

sample exhibited fluid-like properties. Moreover, a third sample containing 50 g L^{-1} triblock terpolymer micelles formed a free-standing gel in a simple test tube inversion experiment due to enhanced interparticular correlations.

In order to understand the liquid structure in more detail, the particle-averaged total correlation function $h_{OP}(\boldsymbol{q})$ defined in eqn (5) has been calculated using the polymer reference interaction site integral equation theory (see ref. 48 and references therein). In contrast to the successful application of this theoretical approach to various polymer nanoparticles,[43,45–47,49] it was not possible to achieve such good agreement between the integral equation theory for the rigid patchy cylinders shown in Fig. 2(b) and the experimental data sets across the entire q-range and for all scattering length contrasts given by the symbols in Fig. 4(a). The differences between the measured and calculated results may be due to a number of possible factors with the most critical being the model assumption that the PS and PMMA polymer chains form a rigid biphasic shell. Due to molecular flexibility, the contribution to the scattering features from intermolecular PS and PMMA correlations is less pronounced than the corresponding one of a rigid biphasic shell.

Having observed that the integral equation theory for the initial rigid patchy cylinders did not lead to a good description of all available scattering data, only contributions to the particle-averaged total correlation function arising from patchy cylinders with an effective radius R_{eff} = 11.5 nm were considered. The calculated scattering intensities from this model (solid lines in Fig. 4(a)) are comparable to the experimental data. Notably, little overall contribution to the scattering features was observed from the total correlation function in the case of the lowest scattering length density of the solvent (lowest data set in Fig. 4(a)), due to the presence of both positive and negative contributions of the compartments of the triblock terpolymer micelles. The peak at $q \approx 0.1$ nm^{-1} observed for the three upper data sets in Fig. 4(a) can be interpreted as a sign of intermediate range order with a characteristic real space distance of $2\pi/q \approx 63$ nm. Future theoretical work may focus on a detailed understanding of local order in fluids consisting of patchy cylinders.

Finally, we note that the experimentally determined scattering intensities shown in Fig. 4(a) can be split consistently into three parts according to (see ref. 42 and references therein)

$$I_{coh}(\boldsymbol{q}) = (\tilde{b} - b_{solvent})^2 I_S(q) + 2(\tilde{b} - b_{solvent})I_{SI}(q) + I_I(q), \tag{9}$$

where $\tilde{b} \approx 3.2 \times 10^{10}$ cm^{-2} is the average scattering length density of the triblock terpolymer micelles. The first term $I_S(q)$ is the normalized scattering intensity of chemically homogeneous micelles, while $I_I(q)$ is related to the scattering length inhomogeneity of the triblock terpolymer micelles. The cross term $I_{SI}(q)$ between the former contributions can take negative values. In general all three terms can be extracted from experimental data if scattering intensities have been measured at least at three different scattering length densities of the solvent. For the triblock terpolymer micelles under consideration the scattering length density independent term $I_I(q)$ is very similar to the middle data set in Fig. 4(a). Moreover, $I_S(q)$ can be considered as the normalized scattering intensity measured

at infinite contrast, where the last two terms in eqn (9) can be neglected. The functional shape of $I_S(q)$ is similar to the upper data set in Fig. 4(a) for $q \lesssim 0.1$ nm^{-1}.

4 Conclusion

SANS data have been collected for polystyrene-*block*-polyethylene-*block*-poly(methyl methacrylate) triblock terpolymer micelles in organic solvents. The structure of these micelles dissolved in protonated tetrahydrofuran has been elucidated by comparing the experimentally determined scattering intensity to the calculated one for a patchy cylinder (see Fig. 3(b)). Moreover, the theoretical analysis revealed that SANS allows one to distinguish patchy cylinders from Janus cylinders (see Fig. 3(a)). The combined experimental and theoretical study shows the presence of alternating polystyrene and poly(methyl methacrylate) regions in the shell of the patchy, cylindrical triblock terpolymer micelles (see Fig. 2(b)).

It has not been possible to use the polymer reference integral equation theory for rigid patchy cylinders to interrogate the scattering data of the triblock terpolymer micelles at rather high concentration in various mixtures of protonated and deuterated tetrahydrofuran. The principle reason for this may be that the amorphous polystyrene and poly(methyl methacrylate) chains forming the shell of the core–shell micelles require chain flexibility to be taken into account. However, consistent information was obtained by separating the data analysis into two portions, analyzing the scattering data considering noninteracting patchy cylinders (see dashed lines in Fig. 4(a)) and taking into account interparticular correlations from patchy cylinders with an effective shell radius (see solid lines in Fig. 4(a)). Upon further increasing the micelle concentration the SANS data show, categorically, the presence of pronounced interparticular correlations (see Fig. 4(b)).

References

1 S. Förster, *Ber. Bunsenges. Phys. Chem.*, 1997, **101**, 1671.
2 F. S. Bates and G. H. Frederickson, *Phys. Today*, 1999, **52**, 32.
3 I. W. Hamley, S.-M. Mai, A. J. Ryan, J. P. A. Fairclough and C. Booth, *Phys. Chem. Chem. Phys.*, 2001, **3**, 2972.
4 T. Hellweg, in *Self Organized Nanostructures of Amphiphilic Block Copolymers II*, ed. O. Borisov and A. H. E. Müller, Springer, Heidelberg, 2012, p. 1.
5 A.-V. Ruzette and L. Leibler, *Nat. Mater.*, 2005, **4**, 19.
6 J. Rodriguez-Hernandez, F. Checot, Y. Gnanou and S. Lecommandoux, *Prog. Polym. Sci.*, 2005, **30**, 691.
7 N. Haberkorn, M. C. Lechmann, B. H. Son, K. Char, J. S. Gutmann and P. Theato, *Macromol. Rapid Commun.*, 2009, **30**, 1146.
8 M. Motornov, Y. Roiter, I. Tokarev and S. Minko, *Prog. Polym. Sci.*, 2010, **35**, 174.
9 J. K. Kim, S. Y. Yang, Y. Lee and Y. Kim, *Prog. Polym. Sci.*, 2010, **35**, 1325.
10 H.-C. Kim, S.-M. Park and W. D. Hinsberg, *Chem. Rev.*, 2010, **110**, 146.
11 N. Hadjichristidis, H. Iatrou, M. Pitsikalis, S. Pispas and A. Avgeropoulos, *Prog. Polym. Sci.*, 2005, **30**, 725.
12 J. Dupont and G. Liu, *Soft Matter*, 2010, **6**, 3654.
13 J. Z. Du and R. K. O'Reilly, *Chem. Soc. Rev.*, 2011, **40**, 2402.
14 K. Zhang, M. Jiang and D. Chen, *Prog. Polym. Sci.*, 2012, **37**, 445.
15 A. O. Moughton, M. A. Hillmyer and T. P. Lodge, *Macromolecules*, 2012, **45**, 2.
16 A. Walther and A. H. E. Müller, *Soft Matter*, 2008, **4**, 663.
17 A. Walther, K. Matussek and A. H. E. Müller, *ACS Nano*, 2008, **2**, 1167.
18 I. K. Voets, R. Fokkink, T. Hellweg, S. M. King, P. de Waard, A. de Keizer and M. A. Cohen Stuart, *Soft Matter*, 2009, **5**, 999.
19 S. Jiang, Q. Chen, M. Tripathy, E. Luijten, K. S. Schweizer and S. Granick, *Adv. Mater.*, 2010, **22**, 1060.
20 I. Kretzschmar and J. H. Song, *Curr. Opin. Coll. Interface Sci.*, 2011, **16**, 84.
21 R. Erhardt, A. Böker, H. Zettl, H. Kaya, W. Pyckhout-Hintzen, G. Krausch, V. Abetz and A. H. E. Müller, *Macromolecules*, 2001, **34**, 1069.
22 S. C. Glotzer and M. J. Solomon, *Nat. Mater.*, 2007, **6**, 557.
23 A. B. Pawar and I. Kretzschmar, *Macromol. Rapid Commun.*, 2010, **31**, 150.
24 Y. Liu, V. Abetz and A. H. E. Müller, *Macromolecules*, 2003, **36**, 7894.
25 T. M. Ruhland, A. H. Gröschel, A. Walther and A. H. E. Müller, *Langmuir*, 2011, **11**, 9807.
26 P. E. Theodorakis, W. Paul and K. Binder, *Macromolecules*, 2010, **43**, 5137.
27 I. Erukhimovich, P. E. Theodorakis, W. Paul and K. Binder, *J. Chem. Phys.*, 2011, **134**, 054906.
28 P. E. Theodorakis, H.-S. Hsu, W. Paul and K. Binder, *J. Chem. Phys.*, 2011, **135**, 164903.
29 M. Lazzari and A. Lopez-Quintela, *Macromol. Rapid Commun.*, 2009, **21**, 1785.
30 J. Dupont, G. J. Liu, K. Niihara, R. Kimoto and H. Jinnai, *Angew. Chem., Int. Ed.*, 2009, **48**, 6144.
31 X. Wang, G. Guerin, H. Wang, Y. Wang, I. Manners and M. A. Winnik, *Science*, 2007, **317**, 644.
32 T. Gädt, N. S. Ieong, G. Cambridge, M. A. Winnik and I. Manners, *Nat. Mater.*, 2009, **8**, 144.
33 F. He, T. Gädt, I. Manners and M. A. Winnik, *J. Am. Chem. Soc.*, 2011, **133**, 23.
34 J. Qian, M. Zhang, I. Manners and M. A. Winnik, *Trends Biotechnol.*, 2010, **28**, 84.
35 H. Schmalz, J. Schmelz, M. Drechsler, J. Yuan, A. Walther, K. Schweimer and A. M. Mihut, *Macromolecules*, 2008, **41**, 3235.
36 J. Schmelz, M. Karg, T. Hellweg and H. Schmalz, *ACS Nano*, 2011, **5**, 9523.
37 T. Fütterer, A. Nordskog, T. Hellweg, G. H. Findenegg, S. Förster and C. D. Dewhurst, *Phys. Rev. E: Stat., Nonlinear, Soft Matter Phys.*, 2004, **70**, 041408.
38 A. Walther, M. Drechsler, S. Rosenfeldt, L. Harnau, M. Ballauff, V. Abetz and A. H. E. Müller, *J. Am. Chem. Soc.*, 2009, **13**, 4720.
39 C. E. Williams, in *Neutron, X-Ray and Light Scattering*, ed. P. Lindner and T. Zemb, Elsevier Science Publisher, Oxford, 1991, p. 101.
40 N. P. Balsara, D. J. Lohse, W. W. Graessley and R. Krishnamoorti, *J. Chem. Phys.*, 1994, **100**, 3905.
41 *Polymers and Neutron Scattering*, ed. J. S. Higgins and H. C. Benoit, Clarendon Press Ithaca, Oxford, 1996.
42 S. Rosenfeldt, M. Ballauff, P. Lindner and L. Harnau, *J. Chem. Phys.*, 2009, **130**, 244901.
43 S. Yan, L. Harnau, N. A. M. Besseling, A. de Keizer, M. Ballauff, S. Rosenfeldt and M. A. Cohen-Stuart, *Soft Matter*, 2008, **4**, 2207.
44 K. Henzler, S. Rosenfeldt, A. Wittemann, L. Harnau, S. Finet, T. Narayanan and M. Ballauff, *Phys. Rev. Lett.*, 2008, **100**, 158301.
45 C. N. Rochette, S. Rosenfeldt, K. Henzler, F. Polzer, M. Ballauff, Q. Tong, S. Mecking, M. Drechsler, T. Narayanan and L. Harnau, *Macromolecules*, 2011, **44**, 4845.
46 K. Henzler, B. Haupt, S. Rosenfeldt, L. Harnau, T. Narayanan and M. Ballauff, *Phys. Chem. Chem. Phys.*, 2011, **13**, 17599.
47 C. H. M. Weber, A. Chiche, G. Krausch, S. Rosenfeldt, M. Ballauff, L. Harnau, I. Göttker-Schnetmann, Q. Tong and S. Mecking, *Nano Lett.*, 2007, **13**, 2024.
48 L. Harnau, *Mol. Phys.*, 2008, **106**, 1975.
49 S. Bolisetty, S. Rosenfeldt, C. Rochette, L. Harnau, P. Lindner, Y. Xu, A. H. E. Müller and M. Ballauff, *Colloid Polym. Sci.*, 2009, **287**, 129.

12756 | *Phys. Chem. Chem. Phys.*, 2012, **14**, 12750–12756

This journal is © the Owner Societies 2012